ACS NANO

www.acsnano.org

ARTICLE

Aligned Stacking of Nanopatterned 2D Materials for High-Resolution 3D Device Fabrication

Jonas Haas,* Finn Ulrich, Christoph Hofer, Xiao Wang, Kai Braun, and Jannik C. Meyer*

Cite This: *ACS Nano* 2022, 16, 1836–1846

Read Online

ACCESS | Metrics & More | Article Recommendations | Supporting Information

ABSTRACT: **Two-dimensional materials can be combined by placing individual layers on top of each other, so that they are bound only by their van der Waals interaction. The sequence of layers can be chosen arbitrarily, enabling an essentially atomic-level control of the material and thereby a wide choice of properties along one dimension. However, simultaneous control over the structure in the in-plane directions is so far still rather limited. Here, we combine spatially controlled modifications of 2D materials, using focused electron irradiation or electron beam induced etching, with the layer-by-layer assembly of van der Waals heterostructures. The presented assembly process makes it possible to structure each layer with an arbitrary pattern prior to the assembly into the heterostructure. Moreover, it enables a stacking of the layers with accurate lateral alignment, with an accuracy of currently 10 nm, under observation in an electron microscope. Together, this enables the fabrication of almost arbitrary 3D structures with highest spatial resolution.**

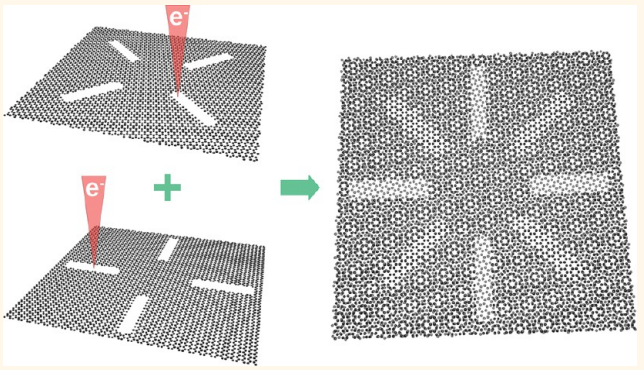

KEYWORDS: *2D materials, van der Waals heterostructures, nanopatterning, electron microscopy, nanoscale assembly, 3D printing*

Structuring matter on the smallest dimensions is a key capability for many areas of technology, most prominently for information processing but also for sensing, nanofluidics, optics, catalysis, medicine, and many more.[1−6] As an observation that has become known as Moore's law,[7,8] the feature sizes in information processing devices have continuously shrunk over many decades, now approaching limitations given by the granularity of the atomic structure. However, current computing devices are essentially planar. Methods for generating arbitrary 3D structures are commonly referred to as "3D printing". Also in this area, the minimum feature sizes that can be defined are continuously shrinking as methods are invented and developed, although the 3D resolution is still larger than what can be achieved in planar structures.[9−14] Currently, optical methods can be pushed to a resolution of about 100 nm.[12] Electron- or ion-beam induced deposition can reach a resolution in the nanometer-range for planar structures on thin membranes,[15] but generally the resolution is limited by the interaction volume rather than the beam diameter, which also depends on the target geometry, and for 3D structures is typically in the range of 10s of nanometers.[11] Another important aspect for 3D printing techniques is the (often rather limited) choice of the materials that can be integrated with each other for fabricating functional devices.[16]

Two-dimensional materials (2D materials) are isolated, one unit cell (or half a unit cell) thick layers, most of which can be described as an individual plane extracted from a van der Waals bonded layered material.[17−21] Some of them are only one atom thick (e.g., graphene or single-layer hexagonal boron nitride), while many more examples can be given for structures with two, three, or more atomic layers. Importantly, these layers can be assembled in any arbitrary sequence, yielding so-called van der Waals (vdW) heterostructures.[20−32] This allows combining the properties of the constituent layers, and may also lead to unique features due to the interaction between the layers. For example, hexagonal boron nitride (hBN) is not only an excellent substrate for graphene,[33] but can also have a

Received: October 15, 2021
Accepted: January 7, 2022
Published: February 2, 2022

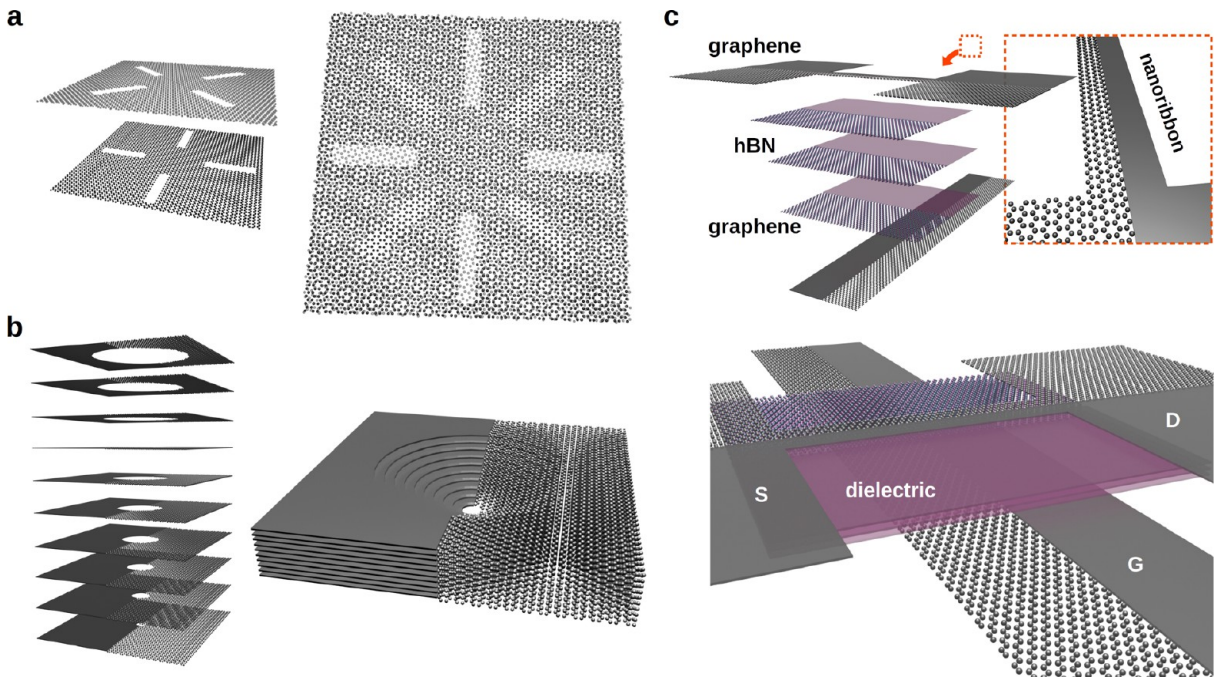

Figure 1. Formation of arbitrary 3D structures by the assembly of prepatterned 2D material layers. (a,b) Illustration of test structures shown in this work, namely (a) two rotated crosses and (b) a nanoscale funnel built from holes of increasing size. (c) Hypothetical transistor structure consisting of graphene leads, a graphene nanoribbon as active element, hBN gate dielectric, and a graphene gate electrode.

profound influence on graphene's electronic properties that sensitively depends on the relative alignment[34,35] of the sheets. The assembly of conducting (e.g., graphene) insulating (e.g., hBN) and semiconducting layers (e.g., molybdenum disulfide, MoS_2) has led to a wide range of device geometries such as transistors with ultrathin gate dielectric,[36] tunneling transistors,[23] memory devices,[37] oscillators,[38] phototransistors,[39] and photovoltaic devices.[40] Modifications of the electronic structure often rely on Moiré effects or other naturally occurring short-range periodicities,[41] with a prominent example being the superconductivity observed in graphene bilayers with a magical misorientation angle of 1.1°.[42] Moiré lattice potentials provide an easy access to periodic variations in the few-nm range, however, they can not be directly used to fabricate more complex potential landscapes. Besides electronic and optical applications, vdW heterostructures are important for molecular sieves,[43] nanopores,[44] catalysis,[45] or nanoscale liquid cells,[46] just to name a few.

2D materials can be structured by conventional lithographic techniques, after they are deposited on a substrate.[47,48] However, much higher resolution can be achieved if 2D materials are available as free-standing membranes: In particular, the direct cutting of graphene,[49−52] other 2D materials,[53,54] or complete vdW heterostructures[55,56] by the focused electron beam in a transmission electron microscope (TEM) or scanning transmission electron microscope (STEM) makes it possible to define feature sizes in the nanometer range. Similarly, electron-beam induced etching (EBIE)[57,58] or cutting of 2D materials by ion beams[59,60] is preferentially done with free-standing membranes. Individual impurity atoms in graphene membranes can even be relocated to specific atomic sites,[61−63] enabling a true atomic-level control, comparable to the relocation of atoms on surfaces using scanning tunneling microscopy.[64] However, again these structures are limited to two dimensions, and the integration with other materials, for example, additional nanostructured layers, is not straightforward.

In this work, we developed an approach that combines the high-resolution, electron-beam based structure definition in free-standing 2D material membranes with the assembly of prestructured layers into van der Waals heterostructures. Figure 1 schematically illustrates the idea: A structure is defined in every one- or few-atom thin layer, and the layers are placed on top of each other with a precise lateral alignment. We categorize this as a form of 3D printing, which (in most of its implementations) also proceeds by forming a target structure layer by layer, and with a chosen arbitrary structure in each individual layer. Critically, the lateral alignment between the layers must be of a similar accuracy than the targeted resolution. Here, we repeatedly achieve an accuracy of about 10 nm, which is given by limitations of the SEM stage control during manual stacking, and probably is not the fundamental limitation of the approach. We also point out that the material for each layer can, in principle, be chosen from the vast repertoire of available 2D materials, which should make it possible to directly create functional devices.

RESULTS AND DISCUSSION

General Considerations. To enable structured modifications by focused electron irradiation at highest resolution, it is essential that the individual layers are free-standing at this step, which is prior to the stacking. Similarly, it is important that the aligned stacking is done with visual feedback from an electron microscope, hence it has to be done in a vacuum (using nanomanipulators). These requirements are in conflict with previously published methods for the deterministic transfer of 2D materials and their assembly into heterostructures,[26−32] all of which employ a transfer medium in contact with the layers, and in some cases a chemical removal of the transfer layer. The concept of our layer transfer is schematically shown in Figure

https://doi.org/10.1021/acsnano.1c09122
ACS Nano 2022, 16, 1836−1846

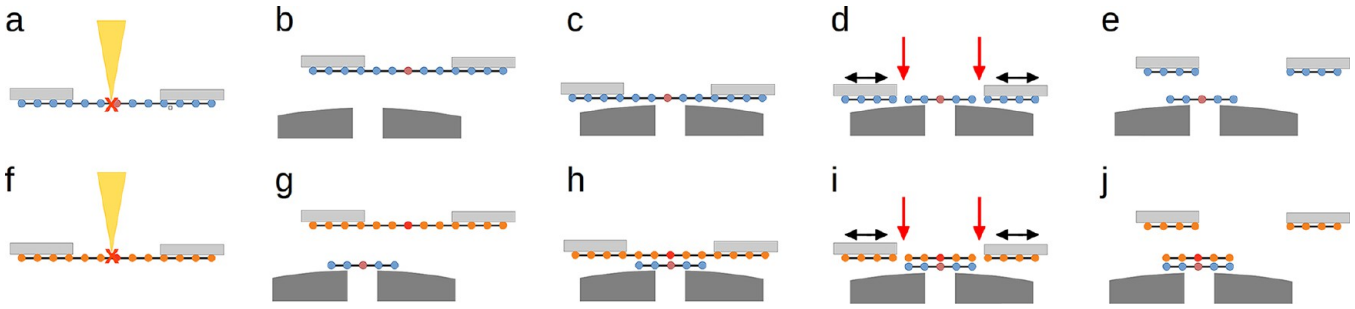

Figure 2. Schematic of the stacking process. (a) The 2D material, which spans a hole in the support frame (e.g., TEM grid), is patterned by focused electron irradiation (modified area indicated as red dot). (b,c) The membrane is moved (under SEM observation) onto a second support with a smaller hole. A slight curvature of the second support frame makes it possible to bring the two surfaces into contact at the desired point. (d) Lateral motion of the support frames relative to each other (black arrows) leads to a rupture of the membrane around the edges of the larger hole (red arrows). (e) Upon separation of the support frames, part of the 2D material stays on the target frame. (f–j) The process is repeated with additional layers, resulting in a stack of 2D material layers.

2: We start with a 2D material layer as free-standing membrane, attached to a relatively large support frame (10 μm diameter in our case). Into this membrane, a pattern is written using focused electron irradiation in the (S)TEM, or by EBIE in the scanning electron microscope (SEM). The membrane is brought into contact with a second, smaller support frame. The surface around this second hole is curved, to facilitate a contact at the desired area in spite of unavoidable small tilt between the two frames. Upon contact, the 2D material membrane sticks to the surface of the smaller support frame, and spans the hole in this frame. Importantly, this adhesion is strong enough that the material can be detached from the initial frame: By moving the initial support frame slightly sideways (black arrows in Figure 2d), the material breaks off from this frame around the edges (red arrows in Figure 2d). Now, the process can be repeated with the next layer (Figure 2f–j).

Implementation. After introducing the concept, we now show the practical implementation. So far, we have prepared stacks of patterned Tungsten disulfide (WS_2), Molybdenum disulfide (MoS_2), and graphene. These 2D materials are prepared into free-standing membranes, and patterns are written into the membranes. For writing patterns into the WS_2 or MoS_2, we used a 200 kV electron beam in a (S)TEM. For graphene, we alternatively use EBIE for removing material in a controlled pattern. This is done using a 3 kV electron beam in a scanning electron microscope in the presence of water vapor (see Methods for details). While EBIE has less spatial resolution than sputtering at high voltages, it requires less time for structuring larger areas. Moreover, it simplifies the process as it can be done in the same device as the stacking. Figure 3 shows exemplary free-standing membranes patterned by EBIE and STEM, respectively.

Now we turn to the most critical aspect of placing and stacking the 2D materials with precise lateral alignment. An illustration of the experimental setup with the manipulation stages, which is used to carry out the presented process (except for patterning individual layers) is shown in Figure 4a. The individual layers are attached to a TEM grid, cut into one-quarter. The target substrate is made from one of the fingers in a FIB lift-out grid, by making it more narrow, making it thinner, and inserting a hole. This is done by FIB, prior to placing the 2D materials, as shown in the Supporting Information (SI). For accurate alignment, the suspended, prestructured layers on the TEM grid are held in a

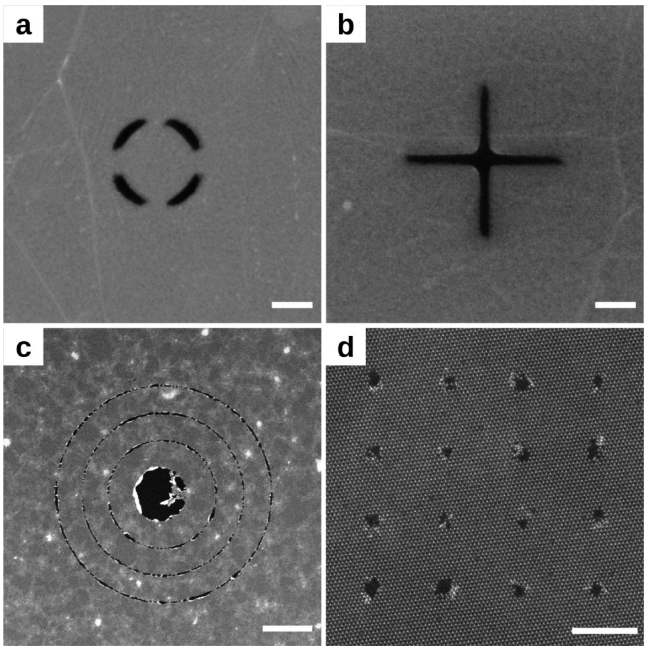

Figure 3. Examples of patterning the free-standing membranes on the initial support frame before stacking. (a,b) H_2O assisted EBIE is used to pattern large features into graphene. (a) Four circular segments and (b) a cross are introduced. (c,d) More filigree patterns can be created using STEM. (c) The image shows a hole with concentric rings patterned into a MoS_2 membrane. (d) A regular array of 0.5–1 nm sized holes is introduced into WS_2 by means of an aberration-corrected STEM. Scale bars are (a,b) 500 nm, (c) 50 nm, and (d) 5 nm.

nanomanipulator which is attached to the SEM chamber. The target substrate is mounted on the six-axis SEM stage.

A schematic image sequence of the process is shown in Figure 4a–f. First, the grid is brought above the target substrate, such that the free-standing membrane is centered on the hole in the target (see Figure 4b–d). Now, the target substrate is moved upward until a contact is made. The contact can be noticed by a clear change in contrast as illustrated in Figure 4e. Slight lateral motion of the TEM grid leads to a rupture of the 2D material at the edge of its connection to the TEM grid. Breaking points, as shown in Figure 4c-f as circular cutouts, can be introduced (already during patterning) to promote tearing-off. Now, the TEM grid can be moved

https://doi.org/10.1021/acsnano.1c09122
ACS Nano 2022, 16, 1836–1846

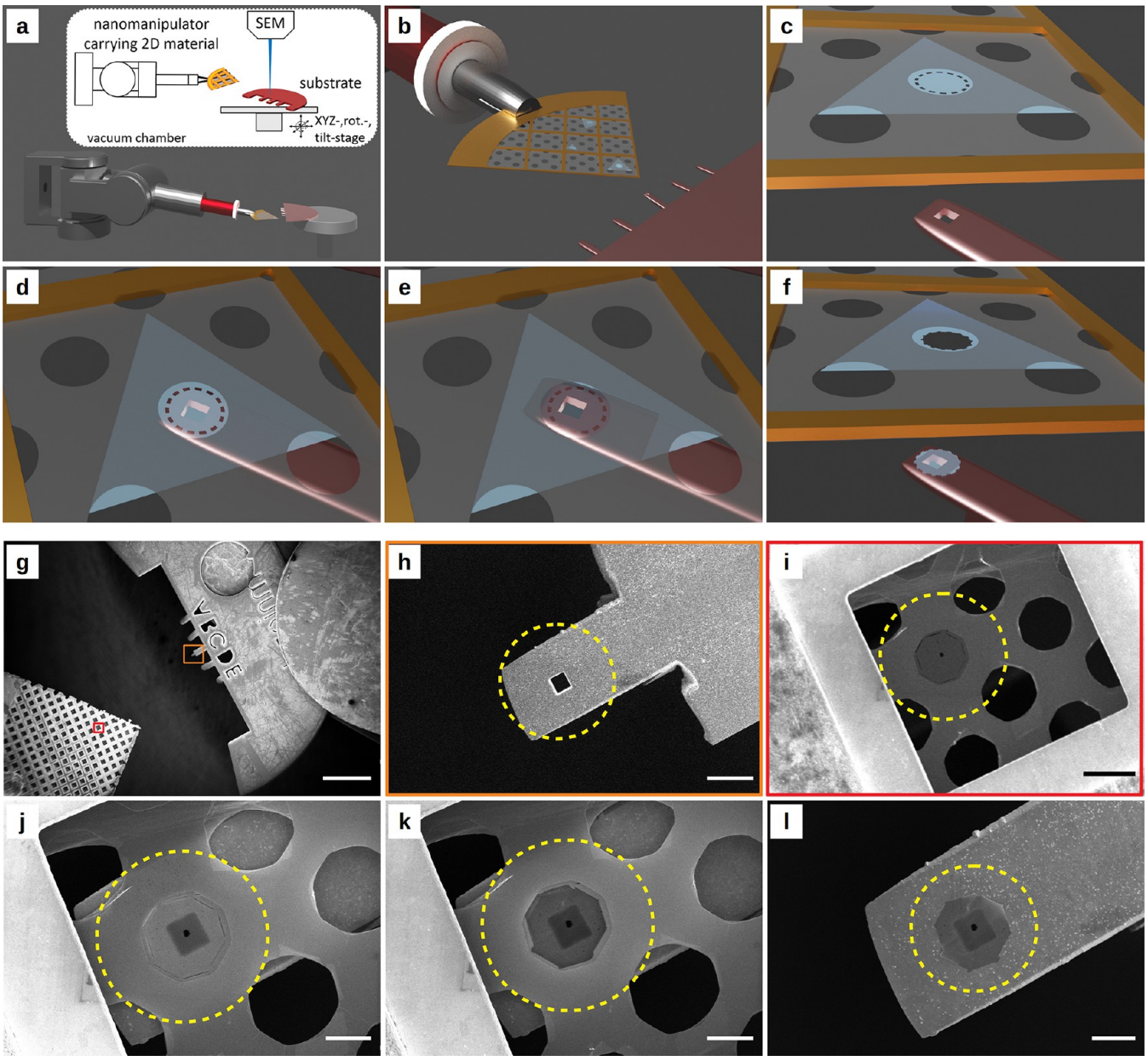

Figure 4. Controlled placement of a 2D material layer. (a–f) Schematic illustration of the procedure and (g–l) SEM images of the process (please see also SI Video). (a,b,g) A quarter of a TEM grid carrying the 2D material is clamped into a nanomanipulator (left). The target substrate, one finger of a FIB lift-out grid (b,g right, c bottom) that was further cut into the desired shape by FIB, is mounted on the *six*-axis SEM stage. (c–e, i–k) One of the 10 μm diameter holes in the grid, spanned by the structured 2D material, is located above the hole in the target frame and brought into contact. (f,l) The membrane breaks off from the TEM grid and remains on the target substrate. (h,i) show close-ups of the regions indicated by the respective color in (g), and the yellow dashed circle in (h,i) indicates the regions that are brought into registry. Scale bars are (g) 500 μm, (h,i) 10 μm and (j–l) 5 μm.

upward, leaving the membrane placed into the desired specific location on the target substrate (Figure 4f).

Figure 4g,l shows an SEM image sequence of placing one graphene membrane. A close-up of the target substrate is shown in Figure 4h, while Figure 4i shows the membrane into which a hole was cut by EBIE suspended on the TEM grid. The grid is brought close to the target substrate, such that the hole in the graphene is centered on the hole in the target. As described above, the membrane is placed by bringing the membrane and the target in contact, notably by a change in the SEM image contrast (see Figure 4j vs Figure 4k and SI Video). Now, the membrane is torn off by slight lateral motions. Importantly, this motion does not cause any displacement of the membrane with respect to the substrate as their adhesion is strong enough, but only rupturing from the TEM grid at the predetermined breaking points. Figure 4l shows the graphene layer after placement on the target substrate. This process is repeated for placing additional layers onto the first one. A video showing the aligned stacking of two patterned graphene layers is given in the SI.

Since the 2D materials are semitransparent in SEM, features in both layers can be observed during placement of a layer, and hence an accurate alignment using the nanomanipulator is possible. It is worth noting that this applies both to the exact

https://doi.org/10.1021/acsnano.1c09122
ACS Nano 2022, 16, 1836–1846

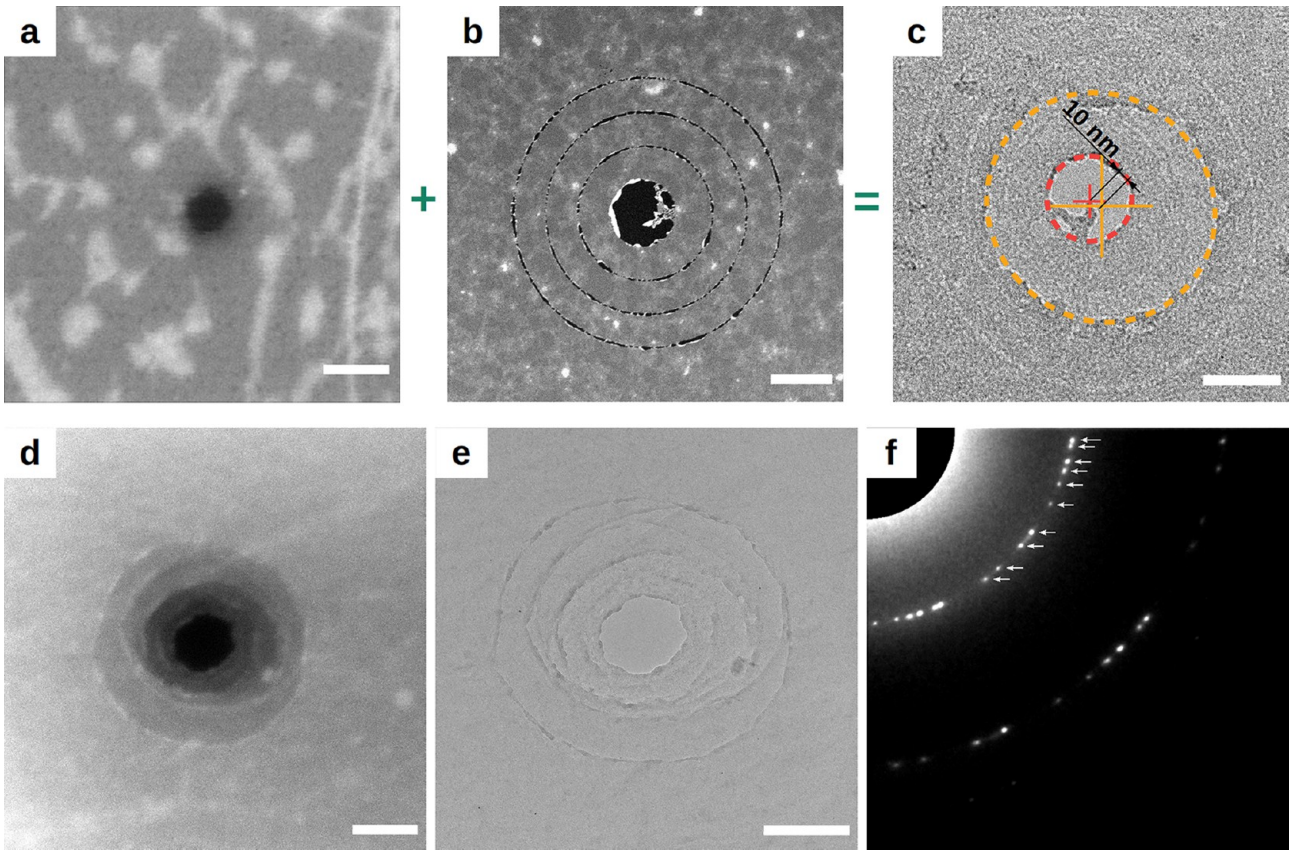

Figure 5. Examples of the layer-by-layer assembly. (a−c) Assembly of patterned graphene and MoS_2 membrane. (a) Hole in graphene, made by EBIE. (b) Central hole and concentric circles in MoS_2, made by sputtering in the STEM. (c) TEM image after aligned placement of the two structures (the slightly elliptical shape of the ring pattern is due to a distortion from an incomplete image corrector alignment). For illustration, the hole in graphene and in MoS_2 are marked in orange and red, respectively. The offset (distance between the centers of the holes) in this case is 10 nm. (d−f) Assembly of 10 graphene layers forming a funnel. Each layer was patterned by EBIE before stacking with holes of different sizes and then stacked in sequence of increasing hole size. (c) shows the SEM and (d) TEM image of the assembly. In the diffraction pattern (f), the arrows indicate the 10 different layers. SEM images after each assembly step with the respective offset are given in SI Figure S2. Scale bar is (a) 200 nm, (b,c) 50 nm and (d,e) 200 nm.

alignment of the membranes to each other as well as of the membranes on the substrate itself. While the layers are still at a distance, they can also be distinguished by the difference in focus height of the SEM (see SI Video). For rough alignment, the secondary electron (SE) or the Inlens-SE detector of the SEM can be used. The combination of the Inlens-SE detector with a STEM detector, however, facilitates the observation of features in the already deposited layers for an accurate alignment. Figures 5 and 6 show SEM and TEM images of layer structures prior to stacking and after stacking.

In order to assess the accuracy of the lateral alignment, we analyze the offset between the patterns of the membranes in the final assembled structure. For this purpose, we measure the distance between the centers of the hole patterns, as exemplified in Figure 5c. Here, the offset between the hole in graphene and the hole in MoS_2 is displaced by about 10 nm. For the assembly of the ten graphene layers (see Figure 5d−f), the average offset was 17 nm, with a minimum of 7 nm and a maximum of 35 nm (see also SI Figure S2).

Integrating Noncontiguous Layer Structures. As for many types of 3D printing, a limitation of the possible structures arises from the requirement that the structures must be stable at any time during the fabrication, that is, already when the structure is only partly finished. In the approach as described so far, even every layer must be stable by itself (as it is separately transferred), which means it can not contain isolated blocks of the material.

To our surprise, however, it turns out that even structures that contain isolated blocks of material can be written into the TMDs, resulting in a "nearly" free-standing structure held only by very thin, disordered residue of material. Some examples are shown in Figure 7: Depending on the sequence of writing the pattern, the isolated block of the TMD may remain at its original position, or may shift to one side. However, we have never observed that the isolated block of the TMD materials disappeared entirely. In Figure 7b, the remaining structure is only supported by a few atom thick strings, which appear to be similar to the wires between beam-induced holes shown in refs 65 and 66. Indeed, as noted already in ref 65 and 66, these wires are much more resistant to damage from the electron beam than the original TMD lattice. Hence, the process of cutting isolated blocks into TMDs becomes self-limiting at the point where the structure is only hanging on few-atom thick wires of the TMD, and thus can be reproduced reliably. For graphene, in this example structured by EBIE, it is similarly possible to create almost-disconnected pieces of material (Figure 7c). However, in this case, the electron dose must be carefully balanced. Pieces of graphene that are disconnected from the support tend to fold up or adhere next to the hole (SI Figure S3).

https://doi.org/10.1021/acsnano.1c09122
ACS Nano 2022, 16, 1836−1846

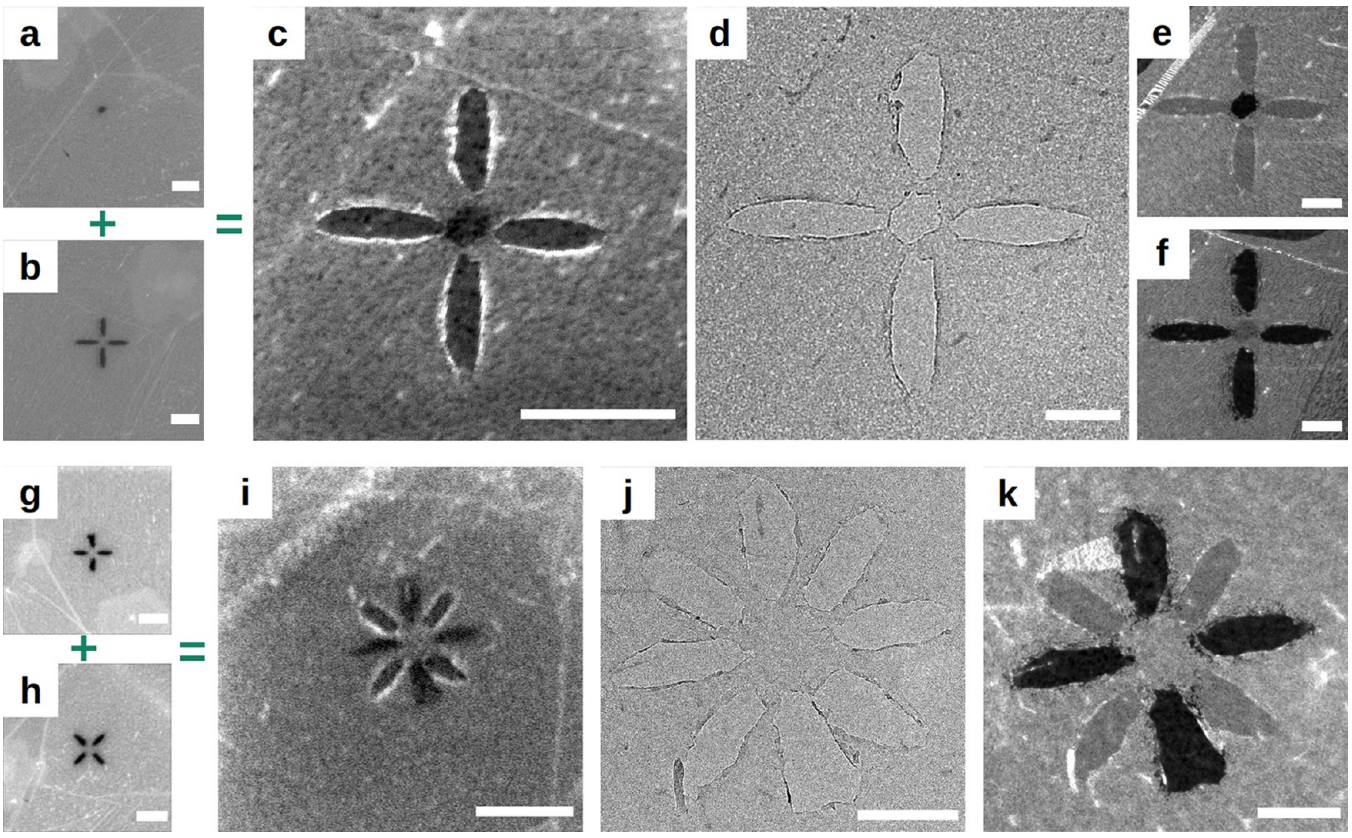

Figure 6. Examples of the layer-by-layer assembly. (a–f) Crosshair built from two graphene layers patterned by EBIE in the SEM with (a) a hole and (b) a cross. (c) SEM and (d) TEM image of the assembly. (e) and (f) are darkfield TEM images highlighting the different lattices of the respective layers. (g–k) Assembly of two crosses patterned in graphene by EBIE. (g) and (h) showing SEM images after patterning the membranes. The resulting stack is shown in (i–k) as SEM, TEM and darkfield TEM image (highlighting one of the two layers), respectively. The 45° relative angle between the two crosses as defined in the individual layers (g,h) is also maintained upon stacking (i–k). Scale bar is (a–c, g–i) 500 nm, (d–f,j,k) 200 nm.

Even delicate structures as in Figure 7b, where a piece of material is only attached by atomic-scale wires, can be assembled into a stack. This is exemplified in Figure 8. After patterning, the almost-isolated WS_2 quantum dot is stacked on top of another WS_2 membrane. Figure 8b shows the resulting structure. To illustrate the individual layers, Fourier filtering is used to highlight the two different lattice orientations in the atomically resolved image. As shown in Figure 8b, one of the layers is continuous, while the other layer contains an isolated disc of WS_2.

Discussion. In this work, we have demonstrated an aligned stacking of prepatterned 2D material layers, which extends the capabilities for in-plane structuring of free-standing layers into the third dimension. Although only three different materials were tested so far, the basic approach can be expected to work with a large variety of 2D materials and possibly other thin layers, for fabricating 3D nanostructures and device geometries.

Most of the graphene patterning within this work was done by EBIE, for the practical reason that it could be done within the same instrument as the stacking. However, the TMD examples were patterned by using an aberration-corrected STEM, which can be performed with nm-scale precision, as evidenced in Figure 3d, and also in prior works.[49−56] We also note that the WS_2 in Figure 3d stays pristine at the regions where no electron dose has been applied, except the one for imaging. This demonstrates how powerful direct patterning in STEM is for high-precision modifications of the 2D material. Moreover, we found that when structuring TMDs by focused, high-energy electron irradiation, one can create isolated blocks of material that are only held in place by a few atomic-scale wires through a self-limiting process. This could be useful to create quantum dot structures out of these materials, or other types of isolated elements in the future.

The patterning in the STEM was carried out at an acceleration voltage of 200 kV. If we consider a displacement threshold of T_d = 6.5 eV for the sulfur atoms in MoS_2 or WS_2[67] and the McKinley-Feshbach formula for a static lattice, the cross section for displacement of the sulfur atom is 160 barn (the static lattice approximation can be used here, since the 200 keV electron energy is far above the knock-on threshold). With a unit cell area of $8.6 \times 10^{-20} m^2$ (almost identical for MoS_2 or WS_2), this translates into a probability of $p = 3.7 \times 10^{-7}$ for one 200 keV electron to knock out one of the sulfur atom from the pristine lattice. Since this cross section is in excellent match to the dose of ca. 2×10^7 electrons per nm^2 that we found was required for cutting MoS_2 or WS_2, we conclude that the beam damage at 200 kV is well explained by knock-on damage. Also, the cross section of 160 barn is far above the ca. 5 barn displacement cross section measured at 20−80 keV in ref 67, which can be considered as representing damage mechanisms other than knock-on.

Stacking of 2D material layers naturally generates an atomic level control over the material sequence along the third

https://doi.org/10.1021/acsnano.1c09122
ACS Nano 2022, 16, 1836−1846

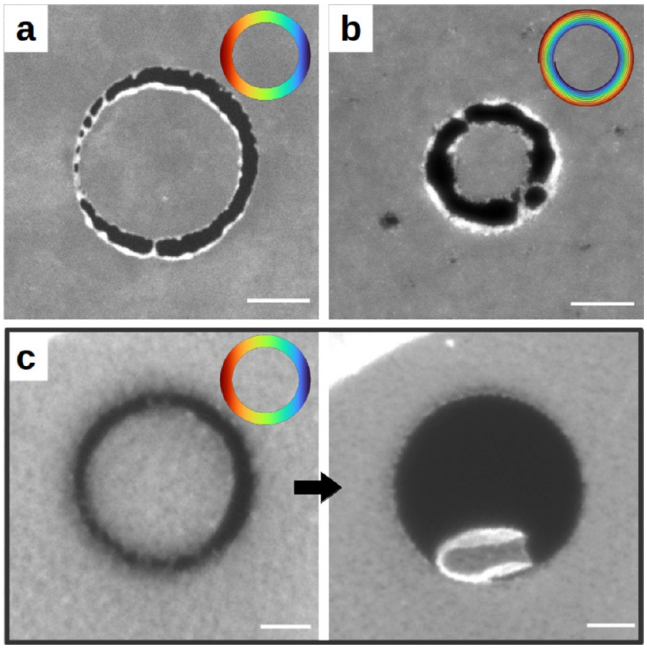

Figure 7. Examples for patterning "nearly" free-standing discs. (a,b) TMD membranes are introduced by sputtering in STEM. The sequence of writing is illustrated by the colored circles with writing from blue to red. (a) The circle is written column by column from right to left resulting in a shifted disc. In (b), the circle is written spirally from the inside to the outside. Here, the disc remains supported only by three small wires. (c) Patterning graphene by EBIE with the same writing sequence as in (a). This also leads to a shifted disc (left image). If more dose is applied, disc detaches from the support and folds up (right image, see also SI Figure S3 for intermediate steps). Scale bar is (a) 20 nm, (b) 5 nm, and (c) 250 nm.

dimension, via the choice of the material, and here also via the potential introduction of gaps in the chosen layers. In this respect, it should be pointed out that in both TEM and SEM imaging of 2D materials, some amount of amorphous carbon is deposited on the 2D materials. This amorphous carbon likely stems from hydrocarbons adsorbed on the sample surfaces which are cracked under electron irradiation. With our experiments carried out in standard TEM and SEM instruments, it is inevitable that these hydrocarbon deposits are also present in the 2D material stacks, including between the layers. Amorphous carbon as formed under an electron beam is not mobile enough to be pushed into pockets of the heterostructure, unlike other contaminants.[24,68] Moreover, in addition to contamination buildup, carbon structures (graphene) are also affected by beam-induced etching even when the water is not intentionally introduced into the chamber. It turned out, that the holes in graphene are enlarged under every e-beam exposure, in particular after the sample has been exposed to air in the transfer between different setups (see SI Figure S4). Patterns in TMDs, however, are not affected, consistent with the impossibility to cut them by water-assisted EBIE (see SI Figures S5 and S6). Further improvements to avoid both the contamination and undesired etching, by carrying out the stacking in an ultrahigh vacuum SEM and structuring the sample at elevated temperature, are currently being set up.

The largest remaining uncertainty in the spatial control over the 3D structure is the accuracy in the lateral alignment of the layers. We regularly achieve an alignment accuracy of about 10 nm, which is slightly less than what one would expect considering the resolution of the SEM of 2−3 nm. The reason is that, currently, the alignment of the layers to each other is only visually estimated by the user while stacking: during the continuous upward movement of the substrate on the Z-stage, the alignment is verified by adjusting the focus to different heights, and corrected using the nanomanipulator if necessary. In addition, a short pixel time must be selected to observe the process in real time, resulting in rather noisy images. We expect that this could be significantly improved by measuring the offset in the SEM image, for example, by automated pattern recognition. An additional practical complication when using the SEM stage is a nonperfect decoupling of in-plane (x,y) and height (z) direction, for example, a jump in (x,y) when inverting or when stopping and restarting the z drive direction. In principle, we see no reason why the accuracy in the lateral alignment could not be pushed to the resolution of the observing electron microscope, or even beyond, indeed, measuring the center position of a given reference feature should be possible with a higher accuracy than the resolution of the underlying image.

We tried to estimate the critical vertical distance between two layers before collapsing into contact. By stepwise getting closer, we determined the distance using the electrical focus of the SEM. Due to the large focus depth in SEM, we only could estimate the distance down to ca. 500 nm. However, we believe that the true critical distance at which two layers collapse into contact is significantly smaller. The twist angle between features in different layers can also be considered as part of the in-plane alignment. As shown in Figure 6g−k, the orientation of the two crosses could be made at the desired relative angle of 45 deg. This is achieved by patterning the two layers into different locations on the same grid containing the source material (prior to stacking), and then, relative orientation of the features as defined during writing is maintained. Rotation of the target is also possible, but was not used so far.

In this work, we have stacked up to ten layers, with features in each layer written by EBIE or STEM based sputtering. We argue that the stacking of individually patterned 2D materials could enable 3D printing at atomic resolution, even though this has not been demonstrated here: Patterning 2D materials by aberration-corrected STEM already achieves sub-nanometer precision, and naturally each 2D material layer is only one or a few atoms thick. The alignment accuracy evidently falls short of the atomic-level precision target by an order of magnitude. However, we do not see any fundamental physical limitation of the technique preventing this. Also, a higher degree of automatization would be needed for a routine use. We also consider the time that would be needed for generating 3D structures in this way: We have built structures with lateral dimensions of the features in the order of 100 nm in diameter, and a thickness of 10 graphene layers. This corresponds to a build volume of ca. $3 \times 10^4 \mathrm{nm}^3$. With the manual preparation, structuring and placement, the time needed to create this assembly is ca. 8 h, resulting in a build speed of ca. 1 nm^3/s. However, most of this time is used for loading samples into a device, for microscope alignment, and similar steps. If we consider only the actual writing time in the STEM (e.g., 10 min for the structure in Figure 3c), and allow 5 min for placing the layer onto the stack, one can estimate a possible speed of ca. 10 nm^3/s for this route of 3D structure fabrication. Such a speed could be anticipated if the whole process, including

https://doi.org/10.1021/acsnano.1c09122
ACS Nano 2022, 16, 1836−1846

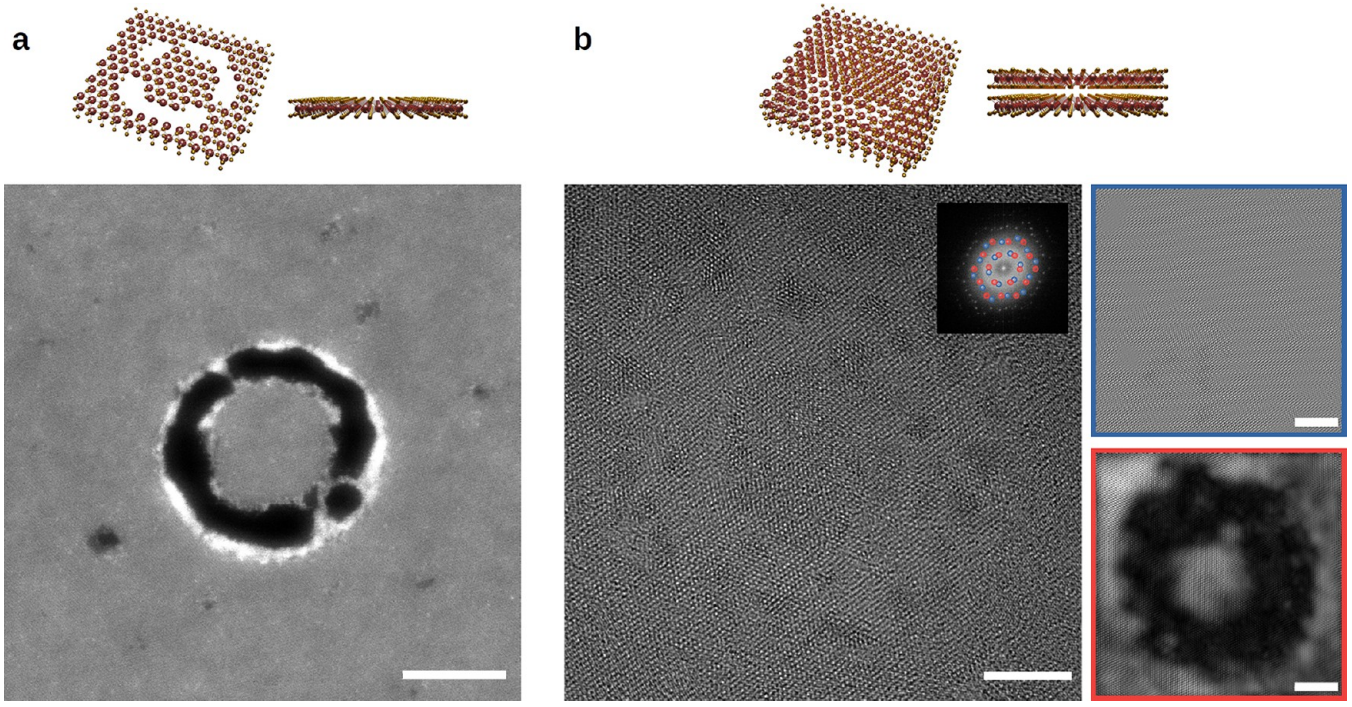

Figure 8. Assembly of noncontiguous structures. (a) A closed ring patterned into a WS_2 membrane (same as in Figure 7b). Small remaining strings support the inner part and allow the fabrication of almost-free features. (b) Stacking of a noncontiguous WS_2 structure on a pristine WS_2 membrane. Fourier filtering of the images is applied to visualize the two individual layers by their different lattice orientations. Scale bar is 5 nm.

sample transfers, is automated. This may still appear slow, but it is actually well on the extrapolated trend for 3D printing speed (volume per unit of time) vs feature size as given in Figure 7 of ref 13.

CONCLUSIONS

We have presented an approach to assemble nanopatterned 2D material layers into multilayer structures, by which features in subsequent layers can be aligned with a lateral offset of ca. 10 nm. The stacking is done in vacuum and under observation of an electron microscope. By the combination of arbitrary structures in each layer and the stacking with precise lateral alignment, it thus becomes possible to create almost arbitrary 3D structures. Moreover, as each layer can be chosen from the large zoo of 2D materials, it should be possible to directly generate a wide variety of functional devices.

METHODS

2D Materials Transfer on TEM Grid. Commercial graphene from Graphenea ("easy transfer" monolayer graphene) is transferred according to the standard protocol of the manufacturer. First, the water-soluble polymer is dissolved in deionized water and the floating sacrificial layer with graphene is fished with the TEM grid (QUANTIFOIL Holey Carbon Films, type R 10/5−10 μm large holes with 5 μm spacing, grid type gold). After drying in air, annealing is performed for 1 h at 150 °C on a hot plate. The sacrificial layer is removed in acetone (50 °C for 1 h) and isopropyl alcohol (1 h).

WS_2 and MoS_2 are grown by chemical vapor deposition on Si/SiO_2 Wafer. The TMD flakes are transferred to the TEM grid (same type as above) following the procedure of ref 69. In short, the grid is placed on the wafer, aligned to the flake and held under light pressure with the help of a micromanipulator (MM3A-EM, Kleindiek). A small droplet of isopropyl alcohol is added on top and the surface tension of the solvent during evaporation ensures contact between the flake and the perforated support film. After annealing on a hot plate (200 °C, 5 min), the silicon oxide of the wafer is etched away in an aqueous solution of potassium hydroxide. Thus, the TEM grid now carrying the TMD flake detaches from the wafer. The sample is then washed in deionized water and isopropyl alcohol and subsequently dried in air.

2D Material Patterning. For patterning the free-standing 2D materials, we use a probe-side aberration corrected JEOL ARM200F or an image-side aberration corrected JEOL ARM200F. Both microscopes are operated in STEM Mode at 200 kV for writing the structures. The digital micrograph (DM) software was used for programming and running a script that controls the beam position such that the desired pattern is written into the membrane. After writing the patterns, initial images are obtained at 200 kV in STEM mode, while avoiding excessive electron doses. Further images are then acquired at 80 kV, using the HRTEM mode on the image-side aberration corrected microscope, or using the STEM mode of the probe-corrected microscope. Typical beam currents are 200pA with a typical dose per area of 3×10^6 C m^{-2} (or ca. 2×10^7 electrons per nm^2) for cutting TMDs.

Alternatively, graphene is patterned (after transfer to the TEM grid) by gas-assisted electron beam induced etching in a Zeiss Leo XB1540 as reported by ref 58. Water vapor is injected near the graphene surface using the gas-injection system of the FIB-SEM (Orsay Physics 5-line GIS). Using an acceleration voltage of 3 kV, the electron beam is scanned over the pattern to be created. Oxidation of graphene by ionized species of the etching agent formed by the electron beam lead to volatile COx products which are removed by the vacuum system.[57] For patterning, a beam current of 3 nA and a typical dose per area of around 5 C m^{-2} is used. Since EBIE can be done in the same SEM as the stacking, this simplifies the process, but the resolution is not as good as patterning by STEM.

Substrate Preparation. A commercially available lift-out grid (Omniprobe, copper with 5 posts) is used as substrate. The outer posts are bent downward whereas the center post is bent upward by about 50 μm. Bending is done by hand using a tweezer and observed in a Zeiss Stemi optical microscope.

Further preparation of the center post is performed by focused ion beam milling in a Zeiss Crossbeam Auriga 40. The tip of the post is

https://doi.org/10.1021/acsnano.1c09122
ACS Nano 2022, 16, 1836−1846

milled narrower to a width of 15 μm and thinner to 5 μm using an acceleration voltage of 30 kV and a milling current of 10 nA. With a lower current of 500 pA, a 2.5 μm × 2.5 μm hole is milled as viewing window in TEM (see also SI Figure S1).

Stack Assembly. The layer assembly is performed in a Zeiss Leo XB1540 equipped with a Kleindiek MM3A-EM nanomanipulator. The TEM grid carrying the 2D material to be stacked is clamped by the manipulator, which is mounted horizontally on the SEM chamber. The lift-out grid as substrate for stacking is held by the SEM six-axis stage. Before loading in the SEM for the assembly, the samples are baked out on a hot plate at 200 °C for 10 min. The SEM is operated at an acceleration voltage of 15 kV to enable the observation of both the membrane to be deposited as well as the target membranes. While the alignment is primarily done with the Inlens-SE detector, it is sometimes useful to also employ the STEM detector of the SEM (images not shown), or a dual-magnification mode that alternately records a normal image and then an image with a smaller field of view (see video in supplement). The latter enables the observation of both the whole support frame as well as introduced features in the membranes in more detail simultaneously.

ASSOCIATED CONTENT

Supporting Information

The Supporting Information is available free of charge at https://pubs.acs.org/doi/10.1021/acsnano.1c09122.

(Preparation of the target substrate, SEM images of 10 layer graphene assembly, SEM images of patterning "nearly" free-standing discs by EBIE, Analysis and discussion of the stability under electron irradiation PDF)

Video of stacking two layers in SEM (AVI)

AUTHOR INFORMATION

Corresponding Authors

Jonas Haas − *Institute of Applied Physics, Eberhard Karls University of Tuebingen, D-72076 Tuebingen, Germany; Natural and Medical Sciences Institute at the University of Tuebingen, D-72770 Reutlingen, Germany;* orcid.org/0000-0001-9964-4364; Email: jonas.haas@uni-tuebingen.de

Jannik C. Meyer − *Institute of Applied Physics, Eberhard Karls University of Tuebingen, D-72076 Tuebingen, Germany; Natural and Medical Sciences Institute at the University of Tuebingen, D-72770 Reutlingen, Germany;* Email: jannik.meyer@uni-tuebingen.de

Authors

Finn Ulrich − *Institute of Applied Physics, Eberhard Karls University of Tuebingen, D-72076 Tuebingen, Germany; Natural and Medical Sciences Institute at the University of Tuebingen, D-72770 Reutlingen, Germany*

Christoph Hofer − *Institute of Applied Physics, Eberhard Karls University of Tuebingen, D-72076 Tuebingen, Germany; Natural and Medical Sciences Institute at the University of Tuebingen, D-72770 Reutlingen, Germany*

Xiao Wang − *School of Physics and Electronics, Hunan University, Changsha, Hunan 410082, China;* orcid.org/0000-0002-2973-8215

Kai Braun − *Institute of Physical and Theoretical Chemistry, Eberhard Karls University of Tuebingen, D-72076 Tuebingen, Germany;* orcid.org/0000-0003-3774-0507

Complete contact information is available at: https://pubs.acs.org/10.1021/acsnano.1c09122

Notes

A prereview version of the manuscript has been posted on the arXiv preprint server: Jonas Haas; Finn Ulrich; Christoph Hofer; Xiao Wang; Kai Braun and Jannik C. Meyer, *Aligned Stacking of Nanopatterned 2D materials − Toward 3D printing at atomic resolution*, 2021, 2110.078 84, arXiv.org, https://arxiv.org/abs/2110.078 84 (accessed December 25, 2021).

The authors declare no competing financial interest.

ACKNOWLEDGMENTS

We acknowledge funding by the Ministry of Science, Research and Art Baden-Württemberg, by the State of Baden-Württemberg, Germany and by the European Union under EU-EFRE grant no. 712 889. We thank B. Schröppel and C. Burkhardt of the NMI for their support on the scanning electron microscopes.

REFERENCES

(1) *Springer Handbook of Nanotechnology*; Bhushan, B., Ed.; Springer: Berlin Heidelberg, 2007.

(2) *Microfabrication for Industrial Applications*; Luttge, R., Ed.; William Andrew Publishing: Boston, 2011.

(3) *Microfluidics and Nanofluidics*; Kandelousi, M. S., Ed.; IntechOpen: London, 2018.

(4) Bocquet, L. Nanofluidics Coming of Age. *Nat. Mater.* **2020**, *19*, 254−256.

(5) *Medical Nanotechnology and Nanomedicine*; Tibbals, H. F., Ed.; CRC Press: Boca Raton, FL, 2017.

(6) Heath, J. R. Nanotechnologies for Biomedical Science and Translational Medicine. *Proc. Natl. Acad. Sci. U. S. A.* **2015**, *112*, 14436−14443.

(7) Schaller, R. R. Moore's Law: Past, Present, and Future. *IEEE Spectrum* **1997**, *34* (52−55), 57.

(8) Mack, C. A. Fifty Years of Moore's Law. *IEEE Trans. Semicond. Manuf.* **2011**, *24*, 202−207.

(9) Engstrom, D. S.; Porter, B.; Pacios, M.; Bhaskaran, H. Additive Nanomanufacturing - A Review. *J. Mater. Res.* **2014**, *29*, 1792−1816.

(10) Farahani, R. D.; Dubé, M.; Therriault, D. Three-Dimensional Printing of Multifunctional Nanocomposites: Manufacturing Techniques and Applications. *Adv. Mater.* **2016**, *28*, 5794−5821.

(11) Hirt, L.; Reiser, A.; Spolenak, R.; Zambelli, T. Additive Manufacturing of Metal Structures at the Micrometer Scale. *Adv. Mater.* **2017**, *29*, 1604211.

(12) Lin, W.; Chen, D.; Chen, S. C. Emerging Micro-Additive Manufacturing Technologies Enabled by Novel Optical Methods. *Photonics Res.* **2020**, *8*, 1827.

(13) Liashenko, I.; Rosell-Llompart, J.; Cabot, A. Ultrafast 3D Printing with Submicrometer Features Using Electrostatic Jet Deflection. *Nat. Commun.* **2020**, *11*, 753.

(14) Jesse, S.; Borisevich, A. Y.; Fowlkes, J. D.; Lupini, A. R.; Rack, P. D.; Unocic, R. R.; Sumpter, B. G.; Kalinin, S. V.; Belianinov, A.; Ovchinnikova, O. S. Directing Matter: Toward Atomic-Scale 3D Nanofabrication. *ACS Nano* **2016**, *10*, 5600−5618.

(15) van Dorp, W. F.; van Someren, B.; Hagen, C. W.; Kruit, P.; Crozier, P.a. Approaching the Resolution Limit of Nanometer-Scale Electron Beam-Induced Deposition. *Nano Lett.* **2005**, *5*, 1303−7.

(16) Deore, B.; Sampson, K. L.; Lacelle, T.; Kredentser, N.; Lefebvre, J.; Young, L. S.; Hyland, J.; Amaya, R. E.; Tanha, J.; Malenfant, P. R.; de Haan, H. W.; Paquet, C. Direct Printing of Functional 3D Objects Using Polymerization-Induced Phase Separation. *Nat. Commun.* **2021**, *12*, 4057.

(17) Novoselov, K. S.; Jiang, D.; Schedin, F.; Booth, T. J.; Khotkevich, V. V.; Morozov, S. V.; Geim, A. K. Two-Dimensional Atomic Crystals. *Proc. Natl. Acad. Sci. U. S. A.* **2005**, *102*, 10451−3.

(18) Mas-Ballesté, R.; Gómez-Navarro, C.; Gómez-Herrero, J.; Zamora, F. 2D Materials: To Graphene and Beyond. *Nanoscale* **2011**, *3*, 20−30.

(19) Das, S.; Robinson, J. A.; Dubey, M.; Terrones, H.; Terrones, M. Beyond Graphene: Progress in Novel Two-Dimensional Materials and Van Der Waals Solids. *Annu. Rev. Mater. Res.* **2015**, *45*, 1−27.
(20) Novoselov, K. S.; Mishchenko, A.; Carvalho, A.; Castro Neto, A. H. 2D Materials and Van Der Waals Heterostructures. *Science* **2016**, *353*, 9439.
(21) Zeng, M.; Xiao, Y.; Liu, J.; Yang, K.; Fu, L. Exploring Two-Dimensional Materials Toward the Next-Generation Circuits: From Monomer Design to Assembly Control. *Chem. Rev.* **2018**, *118*, 6236−6296.
(22) Ponomarenko, L. A.; Geim, A. K.; Zhukov, A. A.; Jalil, R.; Morozov, S. V.; Novoselov, K. S.; Grigorieva, I. V.; Hill, E. H.; Cheianov, V. V.; Fal'ko, V. I.; Watanabe, K.; Taniguchi, T.; Gorbachev, R. V. Tunable Metal−insulator Transition in Double-layer Graphene Heterostructures. *Nat. Phys.* **2011**, *7*, 958−961.
(23) Britnell, L.; Gorbachev, R. V.; Jalil, R.; Belle, B. D.; Schedin, F.; Mishchenko, A.; Georgiou, T.; Katsnelson, M. I.; Eaves, L.; Morozov, S. V.; Peres, N. M. R.; Leist, J.; Geim, A. K.; Novoselov, K. S.; Ponomarenko, L. A. Field-Effect Tunneling Transistor Based on Vertical Graphene Heterostructures. *Science* **2012**, *335*, 947−950.
(24) Haigh, S. J.; Gholinia, A.; Jalil, R.; Romani, S.; Britnell, L.; Elias, D. C.; Novoselov, K. S.; Ponomarenko, L. A.; Geim, A. K.; Gorbachev, R. Cross-Sectional Imaging of Individual Layers and Buried Interfaces of Graphene-Based Heterostructures and Superlattices. *Nat. Mater.* **2012**, *11*, 764−7.
(25) Geim, A. K.; Grigorieva, I. V. Van Der Waals Heterostructures. *Nature* **2013**, *499*, 419−425.
(26) Kang, K.; Lee, K. H.; Han, Y.; Gao, H.; Xie, S.; Muller, D. A.; Park, J. Layer-By-Layer Assembly of Two-Dimensional Materials into Wafer-Scale Heterostructures. *Nature* **2017**, *550*, 229−233.
(27) Frisenda, R.; Navarro-Moratalla, E.; Gant, P.; Lara, D. P. D.; Jarillo-Herrero, P.; Gorbachev, R. V.; Castellanos-Gomez, A. Recent Progress in the Assembly of Nanodevices and Van Der Waals Heterostructures by Deterministic Placement of 2D Materials. *Chem. Soc. Rev.* **2018**, *47*, 53−68.
(28) Ma, L. P.; Ren, W.; Cheng, H. M. Transfer Methods of Graphene from Metal Substrates: A Review. *Small Methods* **2019**, *3*, 1900049.
(29) Hemnani, R. A.; Tischler, J. P.; Carfano, C.; Maiti, R.; Tahersima, M. H.; Bartels, L.; Agarwal, R.; Sorger, V. J. 2D Material Printer: A Deterministic Cross Contamination-Free Transfer Method for Atomically Layered Materials. *2D Mater.* **2019**, *6*, 015006.
(30) Gant, P.; Carrascoso, F.; Zhao, Q.; Ryu, Y. K.; Seitz, M.; Prins, F.; Frisenda, R.; Castellanos-Gomez, A. A System for the Deterministic Transfer of 2D Materials under Inert Environmental Conditions. *2D Mater.* **2020**, *7*, 025034.
(31) Guo, H. W.; Hu, Z.; Liu, Z. B.; Tian, J. G. Stacking of 2D Materials. *Adv. Funct. Mater.* **2021**, *31*, 2007810.
(32) Quellmalz, A.; Wang, X.; Sawallich, S.; Uzlu, B.; Otto, M.; Wagner, S.; Wang, Z.; Prechtl, M.; Hartwig, O.; Luo, S.; Duesberg, G. S.; Lemme, M. C.; Gylfason, K. B.; Roxhed, N.; Stemme, G.; Niklaus, F. Large-Area Integration of Two-Dimensional Materials and Their Heterostructures by Wafer Bonding. *Nat. Commun.* **2021**, *12*, 1−11.
(33) Dean, C. R.; Wang, L.; Maher, P.; Forsythe, C.; Ghahari, F.; Gao, Y.; Katoch, J.; Ishigami, M.; Moon, P.; Koshino, M.; Taniguchi, T.; Watanabe, K.; Shepard, K. L.; Hone, J.; Kim, P.; Young, A. F.; Meric, I.; Lee, C.; Wang, L.; Sorgenfrei, S.; et al. Boron Nitride Substrates for High-Quality Graphene Electronics. *Nat. Nanotechnol.* **2010**, *5*, 722−726.
(34) Kan, E.; Ren, H.; Wu, F.; Li, Z.; Lu, R.; Xiao, C.; Deng, K.; Yang, J. Why the Band Gap of Graphene Is Tunable on Hexagonal Boron Nitride. *J. Phys. Chem. C* **2012**, *116*, 3142−3146.
(35) Hunt, B.; Sanchez-Yamagishi, J. D.; Young, A. F.; Yankowitz, M.; LeRoy, B. J.; Watanabe, K.; Taniguchi, T.; Moon, P.; Koshino, M.; Jarillo-Herrero, P.; Ashoori, R. C. Massive Dirac Fermions and Hofstadter Butterfly in a Van Der Waals Heterostructure. *Science* **2013**, *340*, 1427−1430.
(36) Lee, G. H.; Yu, Y. J.; Cui, X.; Petrone, N.; Lee, C. H.; Choi, M. S.; Lee, D. Y.; Lee, C.; Yoo, W. J.; Watanabe, K.; Taniguchi, T.; Nuckolls, C.; Kim, P.; Hone, J. Flexible and Transparent MoS2 Field-Effect Transistors on Hexagonal Boron Nitride-Graphene Heterostructures. *ACS Nano* **2013**, *7*, 7931−7936.
(37) Sup Choi, M.; Lee, G. H.; Yu, Y. J.; Lee, D. Y.; Hwan Lee, S.; Kim, P.; Hone, J.; Jong Yoo, W. Controlled Charge Trapping by Molybdenum Disulphide and Graphene in Ultrathin Heterostructured Memory Devices. *Nat. Commun.* **2013**, *4*, 1624.
(38) Mishchenko, A.; Tu, J. S.; Cao, Y.; Gorbachev, R. V.; Wallbank, J. R.; Greenaway, M. T.; Morozov, V. E.; Morozov, S. V.; Zhu, M. J.; Wong, S. L.; Withers, F.; Woods, C. R.; Kim, Y. J.; Watanabe, K.; Taniguchi, T.; Vdovin, E. E.; Makarovsky, O.; Fromhold, T. M.; Fal'ko, V. I.; Geim, A. K.; et al. Twist-Controlled Resonant Tunnelling in Graphene/Boron Nitride/Graphene Heterostructures. *Nat. Nanotechnol.* **2014**, *9*, 808−13.
(39) Roy, K.; Padmanabhan, M.; Goswami, S.; Sai, T. P.; Ramalingam, G.; Raghavan, S.; Ghosh, A. Graphene−MoS2 Hybrid Structures for Multifunctional Photoresponsive Memory Devices. *Nat. Nanotechnol.* **2013**, *8*, 826−830.
(40) Britnell, L.; Ribeiro, R. M.; Eckmann, A.; Jalil, R.; Belle, B. D.; Mishchenko, A.; Kim, Y. J.; Gorbachev, R. V.; Georgiou, T.; Morozov, S. V.; Grigorenko, A. N.; Geim, A. K.; Casiraghi, C.; Neto, A. H. C.; Novoselov, K. S. Strong Light-Matter Interactions in Heterostructures of Atomically Thin Films. *Science* **2013**, *340*, 1311−1314.
(41) Celis, A.; Nair, M. N.; Sicot, M.; Nicolas, F.; Kubsky, S.; Malterre, D.; Taleb-Ibrahimi, A.; Tejeda, A. Superlattice-Induced Minigaps in Graphene Band Structure Due to Underlying One-dimensional Nanostructuration. *Phys. Rev. B* **2018**, *97*, 195410.
(42) Cao, Y.; Fatemi, V.; Fang, S.; Watanabe, K.; Taniguchi, T.; Kaxiras, E.; Jarillo-Herrero, P. Unconventional Superconductivity in Magic-Angle Graphene Superlattices. *Nature* **2018**, *556*, 43−50.
(43) Abraham, J.; Vasu, K. S.; Williams, C. D.; Gopinadhan, K.; Su, Y.; Cherian, C. T.; Dix, J.; Prestat, E.; Haigh, S. J.; Grigorieva, I. V.; Carbone, P.; Geim, A. K.; Nair, R. R. Tunable Sieving of Ions Using Graphene Oxide Membranes. *Nat. Nanotechnol.* **2017**, *12*, 546−550.
(44) Zou, A.; Xiu, P.; Ou, X.; Zhou, R. Spontaneous Translocation of Single-Stranded DNA in Graphene-MoS2 Heterostructure Nanopores: Shape Effect. *J. Phys. Chem. B* **2020**, *124*, 9490−9496.
(45) Ren, K.; Luo, Y.; Wang, S.; Chou, J. P.; Yu, J.; Tang, W.; Sun, M. A Van Der Waals Heterostructure Based on Graphene-Like Gallium Nitride and Boron Selenide: A High-Efficiency Photocatalyst for Water Splitting. *ACS Omega* **2019**, *4*, 21689−21697.
(46) Kelly, D. J.; Zhou, M.; Clark, N.; Hamer, M. J.; Lewis, E. A.; Rakowski, A. M.; Haigh, S. J.; Gorbachev, R. V. Nanometer Resolution Elemental Mapping in Graphene-Based TEM Liquid Cells. *Nano Lett.* **2018**, *18*, 1168−1174.
(47) Stampfer, C.; Güttinger, J.; Molitor, F.; Graf, D.; Ihn, T.; Ensslin, K. Tunable Coulomb Blockade in Nanostructured Graphene. *Appl. Phys. Lett.* **2008**, *92*, 012102.
(48) Jessen, B. S.; Gammelgaard, L.; Thomsen, M. R.; Mackenzie, D. M. A.; Thomsen, J. D.; Caridad, J. M.; Duegaard, E.; Watanabe, K.; Taniguchi, T.; Booth, T. J.; Pedersen, T. G.; Jauho, A. P.; Bøggild, P. Lithographic Band Structure Engineering of Graphene. *Nat. Nanotechnol.* **2019**, *14*, 340−346.
(49) Fischbein, M. D.; Drndic, M. Electron Beam Nanosculpting of Suspended Graphene Sheets. *Appl. Phys. Lett.* **2008**, *93*, 113107.
(50) Song, B.; Schneider, G. G. F. G.; Xu, Q.; Pandraud, G.; Dekker, C.; Zandbergen, H. Atomic-Scale Electron-Beam Sculpting of Near-Defect-Free Graphene Nanostructures. *Nano Lett.* **2011**, *11*, 2247−2250.
(51) Börrnert, F.; Fu, L.; Gorantla, S.; Knupfer, M.; Büchner, B.; Rümmeli, M. H. Programmable Sub-Nanometer Sculpting of Graphene with Electron Beams. *ACS Nano* **2012**, *6*, 10327−10334.
(52) Xu, Q.; Wu, M. Y.; Schneider, G. F.; Houben, L.; Malladi, S. K.; Dekker, C.; Yucelen, E.; Dunin-Borkowski, R. E.; Zandbergen, H. W. Controllable Atomic Scale Patterning of Freestanding Monolayer Graphene at Elevated Temperature. *ACS Nano* **2013**, *7*, 1566−1572.
(53) Liu, K.; Feng, J.; Kis, A.; Radenovic, A. Atomically Thin Molybdenum Disulfide Nanopores with High Sensitivity for DNA Translocation. *ACS Nano* **2014**, *8*, 2504−2511.

https://doi.org/10.1021/acsnano.1c09122
ACS Nano 2022, 16, 1836−1846

(54) Masih Das, P.; Danda, G.; Cupo, A.; Parkin, W. M.; Liang, L.; Kharche, N.; Ling, X.; Huang, S.; Dresselhaus, M. S.; Meunier, V.; Drndić, M. Controlled Sculpture of Black Phosphorus Nanoribbons. *ACS Nano* **2016**, *10*, 5687−5695.
(55) Clark, N.; Lewis, E. A.; Haigh, S. J.; Vijayaraghavan, A. Nanometre Electron Beam Sculpting of Suspended Graphene and Hexagonal Boron Nitride Heterostructures. *2D Mater.* **2019**, *6*, 025032.
(56) Masih Das, P.; Thiruraman, J. P.; Zhao, M. Q.; Mandyam, S. V.; Johnson, A. T.; Drndić, M. Atomic-Scale Patterning in Two-Dimensional Van Der Waals Superlattices. *Nanotechnology* **2019**, *31*, 105302.
(57) Spinney, P. S.; Howitt, D. G.; Collins, S. D.; Smith, R. L. Electron Beam Stimulated Oxidation of Carbon. *Nanotechnology* **2009**, *20*, 465301.
(58) Sommer, B.; Sonntag, J.; Ganczarczyk, A.; Braam, D.; Prinz, G.; Lorke, A.; Geller, M. Electron-Beam Induced Nano-Etching of Suspended Graphene. *Sci. Rep.* **2015**, *5*, 7781.
(59) Bell, D. C.; Lemme, M. C.; Stern, L. A.; Williams, J. R.; Marcus, C. M. Precision Cutting and Patterning of Graphene with Helium Ions. *Nanotechnology* **2009**, *20*, 455301.
(60) Fox, D. S.; Zhou, Y.; Maguire, P.; Oneill, A.; Ócoileaín, C.; Gatensby, R.; Glushenkov, A. M.; Tao, T.; Duesberg, G. S.; Shvets, I. V.; Abid, M.; Abid, M.; Wu, H. C.; Chen, Y.; Coleman, J. N.; Donegan, J. F.; Zhang, H. Nanopatterning and Electrical Tuning of MoS2 Layers with a Subnanometer Helium Ion Beam. *Nano Lett.* **2015**, *15*, 5307−5313.
(61) Susi, T.; Meyer, J. C.; Kotakoski, J. Manipulating Low-Dimensional Materials down to the Level of Single Atoms with Electron Irradiation. *Ultramicroscopy* **2017**, *180*, 163−172.
(62) Dyck, O.; Kim, S.; Kalinin, S. V.; Jesse, S. Placing Single Atoms in Graphene with a Scanning Transmission Electron Microscope. *Appl. Phys. Lett.* **2017**, *111*, 113104.
(63) Tripathi, M.; Mittelberger, A.; Pike, N. A.; Mangler, C.; Meyer, J. C.; Verstraete, M. J.; Kotakoski, J.; Susi, T. Electron-Beam Manipulation of Silicon Dopants in Graphene. *Nano Lett.* **2018**, *18*, 5319−5323.
(64) Crommie, M. F.; Lutz, C. P.; Eigler, D. M. Confinement of Electrons to Quantum Corrals on a Metal Surface. *Science* **1993**, *262*, 218−220.
(65) Liu, X.; Xu, T.; Wu, X.; Zhang, Z.; Yu, J.; Qiu, H.; Hong, J. H.; Jin, C. H.; Li, J. X.; Wang, X. R.; Sun, L. T.; Guo, W. Top-Down Fabrication of Sub-Nanometre Semiconducting Nanoribbons Derived from Molybdenum Disulfide Sheets. *Nat. Commun.* **2013**, *4*, 1776.
(66) Lin, J.; Cretu, O.; Zhou, W.; Suenaga, K.; Prasai, D.; Bolotin, K. I.; Cuong, N. T.; Otani, M.; Okada, S.; Lupini, A. R.; Idrobo, J. C.; Caudel, D.; Burger, A.; Ghimire, N. J.; Yan, J.; Mandrus, D. G.; Pennycook, S. J.; Pantelides, S. T. Flexible Metallic Nanowires with Self-Adaptive Contacts to Semiconducting Transition-Metal Dichalcogenide Monolayers. *Nat. Nanotechnol.* **2014**, *9*, 436−42.
(67) Kretschmer, S.; Lehnert, T.; Kaiser, U.; Krasheninnikov, A. V. Formation of Defects in Two-Dimensional MoS2 in the Transmission Electron Microscope at Electron Energies below the Knock-on Threshold: The Role of Electronic Excitations. *Nano Lett.* **2020**, *20*, 2865−2870.
(68) Purdie, D. G.; Pugno, N. M.; Taniguchi, T.; Watanabe, K.; Ferrari, A. C.; Lombardo, A. Cleaning Interfaces in Layered Materials Heterostructures. *Nat. Commun.* **2018**, *9*, 5387.
(69) Meyer, J. C.; Girit, C. O.; Crommie, M. F.; Zettl, A. Hydrocarbon Lithography on Graphene Membranes. *Appl. Phys. Lett.* **2008**, *92*, 123110.

https://doi.org/10.1021/acsnano.1c09122
ACS Nano 2022, 16, 1836−1846